Highly efficient maternal-fetal Zika virus transmission in pregnant rhesus macaques

Sydney M. Nguyen[1*], Kathleen M. Antony[1*], Dawn M. Dudley[2]*, Sarah Kohn[3], Heather A. Simmons[5], Bryce Wolfe[2], M. Shahriar Salamat[2], Leandro B. C. Teixeira[10], Gregory J. Wiepz[4], Troy H. Thoong[5], Matthew T. Aliota[6], Andrea M. Weiler[5], Gabrielle L. Barry[5], Kim L. Weisgrau[5], Logan J. Vosler[5], Mariel S. Mohns[2], Meghan E. Breitbach[2], Laurel M. Stewart[2], Mustafa N. Rasheed[2], Christina M. Newman[2], Michael E. Graham[2], Oliver E. Wieben[3], Patrick A. Turski[3], Kevin M. Johnson[3], Jennifer Post[5], Jennifer M. Hayes[5], Nancy Schultz-Darken[5], Michele L. Schotzko[5], Josh A. Eudailey[7], Sallie R. Permar[7], Eva G. Rakasz[5], Emma L. Mohr[8], Saverio Capuano III[5], Alice F. Tarantal[9], Jorge E. Osorio[6], Shelby L. O'Connor[2], Thomas C. Friedrich[5, 6], David H. O'Connor[2, 5], and Thaddeus G. Golos[1, 4, 5].

[1]Department of Obstetrics and Gynecology, University of Wisconsin-Madison

[2]Department of Pathology and Laboratory Medicine, University of Wisconsin-Madison

[3]Department of Radiology, University of Wisconsin-Madison

[4]Department of Comparative Biosciences, University of Wisconsin-Madison

[5]Wisconsin National Primate Research Center, University of Wisconsin-Madison

[6]Department of Pathobiological Sciences, University of Wisconsin-Madison

[7]Department of Pediatrics and Human Vaccine Institute, Duke University Medical Center

[8]Department of Pediatrics, University of Wisconsin-Madison

[9]Departments of Pediatrics and Cell Biology and Human Anatomy, University of California-Davis, California National Primate Research Center, Davis, CA

[10]School of Veterinary Medicine, University of Wisconsin-Madison

*These authors contributed equally to this work. Correspondence and request for materials should be addressed to T.G.G. (email: golos@primate.wisc.edu).

Abstract
Infection with Zika virus (ZIKV) is associated with human congenital fetal anomalies. To model fetal outcomes in nonhuman primates, we administered Asian-lineage ZIKV subcutaneously to four pregnant rhesus macaques. While non-pregnant animals clear viremia within 10-12 days, maternal viremia was prolonged in 3 of 4 pregnancies. Fetal head growth velocity in the last month of gestation determined by ultrasound assessment of head circumference was decreased in comparison with biparietal diameter and femur length within each fetus, both within normal range. ZIKV RNA was detected in tissues from all four fetuses at term cesarean section. In all pregnancies, neutrophilic infiltration was present at the maternal-fetal interface (decidua, placenta, fetal membranes), in various fetal tissues, and in fetal retina, choroid, and optic nerve (first trimester infection only). Consistent vertical transmission in this primate model may provide a platform to assess risk factors and test therapeutic interventions for interruption of fetal infection.

Zika Virus (ZIKV; *Flaviviridae, Flavivirus*) is spread by *Aedes* mosquitoes[1,2] and sexual contact[3-9]. ZIKV is now endemic in the Americas following its introduction in 2014. *In utero* infection with ZIKV circulating in Oceania and the Americas has been associated with increased incidence of fetal microcephaly[10,11]. Fetal findings include placental calcifications, growth restriction, arthrogryposis, severe central nervous system (CNS) malformations[10,12-16], intraocular calcifications, cataracts[17,18] and skeletal[19], and sensory[20] disorders. The constellation of developmental abnormalities observed following ZIKV infection during pregnancy is termed "congenital Zika syndrome"[21-23]. Prolonged viremia (>14 days) during pregnancy compared to nonpregnant individuals (7-10 days[24]) has been noted[24-26], however the potential association between prolonged maternal viremia and congenital Zika syndrome is not clear at this time.

Nonhuman primates are important models for human infectious disease, and ZIKV infection in rhesus macaques (*Macaca mulatta*) has been established[27-29]. Viremia in nonpregnant Indian rhesus macaques has been shown to persist for 7-10 days, similar to human infection[27-29]. Nonhuman primate pregnancy has salient similarities to human pregnancy, including hemochorial placentation with extensive trophoblast invasion and remodeling of decidual spiral arteries[30-32], and prolonged gestation with a similar trajectory of fetal development[33]. Maternal infection with a high dose of an Asian viral strain (strain FSS13025, Cambodia 2010) in a single pigtail macaque (*Macaca nemestrina*) resulted in maternal viremia and severe fetal neurodevelopmental abnormalities as well as fetal and placental infection[34].

It was previously reported that while moderate infectious doses of ZIKV are cleared promptly in nonpregnant macaques, initial data from two pregnant macaques infected in the first trimester showed prolonged viremia, similar to reports of human pregnancies[27]. Here we report that the fetuses of these two first trimester ZIKV pregnancies, as well as two additional late second/early third trimester infections, had maternal-fetal ZIKV transmission with vRNA and pathology in fetal tissues as well as at the maternal-fetal interface.

Results

Maternal ZIKV in blood and other body fluids. Four pregnant macaques were infected by subcutaneous injection of $1x10^4$ PFU of the Asian-lineage ZIKV strain H.sapiens-tc/FRA/2013/FrenchPolynesia-3328[27], which is closely related to strains circulating in the Americas. Animals 827577 and 680875 were infected at 31 or 38 days gestation, respectively (mid-first trimester) (term 165±10 days). Animals 598248 and 357676 were infected at 103 or 118 days gestation, respectively (late second/early third trimester). ZIKV RNA was measured in plasma, urine, saliva, and amniotic fluid, and ultrasound imaging of the fetus was performed following infection through ~155 days gestation (Figs. 1a, S1). All monkeys had detectable plasma viremia for 11 to 70 days post-inoculation (dpi) (Figs. 1b, 2a) and at least one day of detectable vRNA in urine. Two macaques had detectable vRNA in saliva, and one macaque infected at the beginning of the third trimester had detectable vRNA in amniotic fluid on 15, 22, and 36 dpi (118, 125, and 139 days gestation, respectively) (Fig. 1b).

Innate and adaptive immune responses to ZIKV. The duration of viremia was prolonged in three of four pregnant macaques in comparison to non-pregnant animals infected by the same route, dose, and strain of ZIKV in a previous study[27] (Fig. 2a; compare colored and gray lines). To evaluate maternal immune responses, peripheral blood CD16+ natural killer (NK) cell and CD95+CD28- CD8 effector T cell proliferation were monitored by flow cytometry for Ki-67 expression. Although responses were variable, there was generally higher proliferation relative to baseline in peripheral blood CD16+ NK cells than in CD95+CD28- CD8+ effector T cells (Fig.

2b), and these responses were not qualitatively different from nonpregnant animals (Fig. 2b, grey tracings). The numbers of circulating plasmablasts tended to increase more slowly in third-trimester infections; however, the response did not distinctly differ between the first and third trimesters (Fig. 2c). Neutralizing antibody titers assessed by $PRNT_{90}$ at 28 dpi did not differ between first and third trimester infections (Fig. 2d). Interestingly, animal 660875 (first trimester infection) had more vigorous and prolonged NK, T cell, and plasmablast responses to infection compared to the other three pregnancies. ZIKV infection was not associated with consistent changes in complete blood cell counts or serum chemistry in pregnant animals (Supplementary Fig. S2).

Assessment of fetal growth. Sonographic images (e.g., Fig. 3a) were obtained approximately weekly to monitor fetal growth and viability. No significant fetal or placental abnormalities were observed. Fetal femur length (FL) was typically within one standard deviation (SD) of mean database values for fetal rhesus macaques across gestation[35], suggesting absence of symmetrical growth restriction (Fig. 3b). The biparietal diameter (BPD) was within two SD of expected values across gestation (Fig. 3c). However, during the last month of pregnancy, head circumference (HC) in all animals was between one and three SD below the mean (Fig. 3d).

To discern changes in fetal growth trajectories, we extrapolated the predicted gestational ages (pGA) by mapping the observed fetal biometric measures in individual pregnancies onto normative growth curves for BPD, FL, and HC[35,36]. Figs. 3e-h compare within each animal the pGA estimated by an average of BPD and FL with that estimated by HC. In 3 of 4 pregnancies, pGA as estimated by HC lagged 16.5 to 19 days behind the pGA estimated by an average of BPD and FL. HC reflects both BPD and occipitofrontal diameters. Human fetuses and infants affected by severe microcephaly in congenital ZIKV infection have vermis agenesis (growth failure of the cerebellum) and reduced frontal cortex growth[10,13,18,37]: regions of the brain where growth deficits will give rise to a reduced occipitofrontal diameter. Fetal Magnetic Resonance Imaging (MRI) was also performed for the dams infected in the first trimester (827577, imaged at 102 dpi [140 days gestation], and 660875, imaged at 60 dpi [91 days gestation]). These images provided evidence of normal volume, cortical thickness, sulcation, and ventricular and extra-axial spaces (Supplemental Fig. S4). However, it has been reported that human infants whose mothers were infected with ZIKV during pregnancy have been born with normal cranial anatomy, but developed microcephaly within 6 months[38]. Thus, further studies focused on macaque postnatal development are warranted.

Fetal viral burden and histopathology. All ZIKV pregnancies progressed without overt adverse outcomes. At 153-158 days gestation, fetuses were surgically delivered, euthanized, and tissues collected. None of the fetuses had evidence of microcephaly or other abnormalities upon gross examination. Approximately 50 fetal and maternal tissues (supplemental Fig. S5) were collected from each pregnancy for histopathology and vRNA by qRT-PCR. Results are summarized in Fig 4. ZIKV RNA was detected in all four fetuses, albeit in different tissues in individual fetuses, and in some maternal tissues including spleen, liver, lymph node, and decidua (Fig. 4A). Notably, the pregnancy with the longest duration of viremia (827577; 70 days viremia (39-109 days gestation) had fetal tissues (optic nerve, axillary lymph node) with the highest vRNA burden. However, the fetus from the short (9 day) duration maternal viremia (119-127 days gestation) also had vRNA in fetal lymph node, pericardium, and lung (Fig. 4a).

Pathologists were blinded to vRNA findings for histology evaluation and scoring (Supplementary Fig. S6; see Supplementary Data S7 for a full listing of pathology findings). The maternal-fetal

interface in all four ZIKV infections presented minimal to moderate suppurative placentitis with variable mineralization and necrosis, as well as minimal to moderate suppurative deciduitis (Fig. 4b, c). Three of four pregnancies had suppurative amnionitis and three of four dams had mild to moderate suppurative splenitis. Histology confirmed normal CNS structures and absence of encephalitis (inflammation) in all four fetuses. Morphologic fetal diagnoses included: suppurative splenitis, suppurative to lymphoplasmacytic hepatitis, suppurative alveolitis (pneumonia), and suppurative lymphadenitis (Supplemental Data. S7). The duration of viremia or trimester of maternal infection did not generally correlate with the severity or distribution of scored fetal pathologies, however it is significant that both fetuses infected during the first trimester, but not the third trimester, had ocular pathology: inflammation of retina, choroid, and optic nerve (Fig. 4c, Supplementary Data S7, Figures S8, S9). A segment of the fetal axillary lymph node with the highest vRNA burden was immunostained for ZIKV. ZIKV NS2B-positive cells were observed in lymph node medullary cords, a subset of which were CD163-positive macrophages (Fig. 4d; Supplementary Figure S10). However not all ZIKV+ cells were CD163+.

Discussion

This study demonstrates that similar to human pregnancy, Indian rhesus macaque fetuses are susceptible to congenital infection following maternal subcutaneous infection with a moderate infectious dose of Asian-lineage ZIKV during the first or late second/early third trimesters. Maternal-fetal transmission in the macaque is highly efficient: 4 of 4 maternal infections resulted in infected fetuses, all pregnancies demonstrated pathology at the maternal-fetal interface and in the fetus, with variable fetal vRNA distribution, similar to observations in human pregnancy. Fetal infection was accompanied by an apparent reduced trajectory of fetal HC in the last month of gestation, without overall fetal growth restriction. While we hypothesize that the duration of maternal viremia correlates with risk for fetal impact, pathology at the maternal-fetal interface and fetal vRNA and pathologies in the pregnancy with the shortest duration of viremia following third trimester infection suggests that the fetus is at risk even with a brief exposure to circulating maternal virus, as reported in human pregnancy[14]. Indeed, our findings are consistent with the emerging picture of congenital Zika syndrome, in which microcephaly is the most severe of a range of potential sequelae. Given the high rate of vertical transmission in our model in the absence of severe developmental defects, it seems possible that there is a higher rate of human *in utero* ZIKV exposure than is currently appreciated, exposures which are not obvious at birth, but may manifest later in postnatal development. Congenital ZIKV infection in macaques provides a tractable and translational model of human disease. Modest fetal neurodevelopmental outcomes with this specific model, while perhaps unexpected, provide an opportunity to further evaluate factors which foster severe fetal developmental impact, such as co-infection or previous exposure to other pathogens, and support the development of strategies to prevent maternal-fetal transmission and reduce fetal virus burden.

Methods:

Study design

Four pregnant rhesus macaques (*Macaca mulatta*) of Indian ancestry were infected subcutaneously with $1x10^4$ PFU ZIKV (Zika virus/H.sapiens-tc/FRA/2013/FrenchPolynesia-01_v1c1; ZIKV-FP) at 31, 38, 104, or 119 days gestation (term 165±10 days). All macaques utilized in the study were free of Macacine herpesvirus 1, Simian Retrovirus Type D (SRV), Simian T-lymphotropic virus Type 1 (STLV), and Simian Immunodeficiency Virus as part of the Specific Pathogen Free (SPF) colony at WNPRC.

Care and use of macaques

All monkeys used in this study were cared for by the staff at the Wisconsin National Primate Research Center (WNPRC) in accordance with the regulations and guidelines outlined in the Animal Welfare Act and the Guide for the Care and Use of Laboratory Animals and the recommendations of the Weatherall report (https://royalsociety.org/topics-policy/publications/2006/weatherall-report/). This study was approved by the University of Wisconsin-Madison Graduate School Institutional Animal Care and Use Committee. Female monkeys were co-housed with compatible males and observed daily for menses and breeding. Pregnancy was detected by ultrasound examination of the uterus at approximately 20-24 days gestation following the predicted day of ovulation. The day of gestation was estimated (+/- 2 days) based on the dams menstrual cycle and previous pregnancy history, observation of copulation, and the greatest length of the fetus at initial ultrasound examination which was compared to normative growth data in this species[35]. Ultrasound examination of the conceptus was performed subsequent to ZIKV infection as described below. For all procedures (i.e., physical examinations, virus inoculations, ultrasound examinations, blood and swab collection), animals were anesthetized with an intramuscular dose of ketamine (10 mg/kg). Blood samples from the femoral or saphenous vein were obtained using a vacutainer system or needle and syringe. The four pregnant macaques were monitored daily prior to and after infection for any physical signs (e.g., diarrhea, inappetance, inactivity, atypical behaviors).

Inoculations

ZIKV strain H/PF/2013 (GenBank: KJ776791), originally isolated from a 51-year-old female in France returning from French Polynesia with a single round of amplification on Vero cells, was obtained from Xavier de Lamballerie (European Virus Archive, Marseille France). The inoculating stock was prepared and validated as previously described[27]. A single harvest of virus with a titer of 1.26×10^6 PFU/mL (equivalent to 1.43×10^9 vRNA copies/mL) was used for all 4 challenges. Animals were anesthetized as described above, and 1 mL of inocula was administered subcutaneously over the cranial dorsum. Post-inoculation, animals were closely monitored by veterinary and animal care staff for adverse reactions or any signs of disease.

Immunophenotyping

The number of activated/proliferating peripheral blood lymphocyte subset cells was quantified using a modified version of our protocol detailed step-by-step in OMIP-028[39] as previously reported[27]. Briefly, 0.1 mL of EDTA-anticoagulated whole blood samples were incubated for 15 min at room temperature in the presence of a mastermix of antibodies against CD45 (clone D058-1283, Brilliant Violet 786 conjugate, 2.5 µl), CD3 (clone SP34-2 Alexa Fluor 700 conjugate, 5 µl), CD8 (clone SK2, Brilliant Violet 510, 2.5 µl), NKG2A/C (clone Z199, PE-Cy7 conjugate, 5 µl), CD16 (clone 3G8, Pacific Blue conjugate, 5 µl), CD69 (clone TP1.55.3, ECD conjugate, 3 µl), HLA-DR (clone 1D11, Brilliant Violet 650 conjugate, 1 µl), CD4 (clone SK3,

Brilliant Violet 711 conjugate, 5 µl), CD28 (clone CD28.2, PE conjugate, 5 µl), and CD95 (clone DX2, PE-Cy5 conjugate, 10 µl) antigens. All antibodies were obtained from BD BioSciences, with the exception of the NKG2A/C-specific antibody, which was purchased from Beckman Coulter, and the CCR7 antibody that was purchased from R&D Systems. The cells were permeabilized using Bulk Permeabilization Reagent (Life Technology), then stained for 15 min with Ki-67 (clone B56, Alexa Fluor 647 conjugate) while the permeabilizer was present. The cells were then washed twice in media and resuspended in 0.125 ml of 2% paraformaldehyde until they were run on a BD LSRII Flow Cytometer. Flow data were analyzed using Flowjo software version 9.9.3.

Plasmablast detection

Peripheral blood mononuclear cells (PBMCs) isolated from four ZIKV-infected pregnant rhesus monkeys at 3, 7, 11, and 14 dpi were stained with the following panel of fluorescently labeled antibodies (Abs) specific for the following surface markers to analyze for plasmablast presence: CD20 FITC (L27), CD80 PE (L307.4), CD123 PE-Cy7(7G3), CD3 APC-Cy7 (SP34-2), IgG BV605 (G18-145) (all from BD Biosciences, San Jose, CA), CD14 AF700 (M5E2), CD11c BV421 (3.9), CD16 BV570 (3G8), CD27 BV650(O323) (all from BioLegend, San Diego, CA), IgD AF647 (polyclonal) (Southern Biotech, Birmingham, AL), and HLA-DR PE-TxRed (TÜ36) (Invitrogen, Carlsbad, CA). LIVE/DEAD Fixable Aqua Dead Cell Stain Kit (Invitrogen, Carlsbad, CA) was used to discriminate live cells. Cells were analyzed exactly as previously described[27].

Complete blood count (CBC) and serum chemistry panels

CBCs with white blood cell (WBC) differential counts were performed on EDTA-anticoagulated whole blood samples on a Sysmex XS-1000i automated hematology analyzer (Sysmex Corporation, Kobe, Japan). CBCs included the following tests: absolute WBC count, absolute counts and percentages for WBC differentials, red blood cell (RBC) count, hemoglobin and hematocrit, RBC indices (mean corpuscular volume, mean corpuscular hemoglobin, mean corpuscular hemoglobin concentration, and red blood cell distribution width), platelet count, and mean platelet volume. Blood smears were prepared and stained with Wright-Giemsa stain (Wescor Aerospray Hematology Slide Stainer; Wescor Inc, Logan, UT). Manual slide evaluations were performed on samples when laboratory-defined criteria were met (absolute WBC count, WBC differential percentages, hemoglobin, hematocrit, or platelet count outside of reference intervals; automated WBC differential counts unreported by the analyzer; and the presence of analyzer-generated abnormal flags). Manual slide evaluations included WBC differential and platelet counts with evaluation of WBC, RBC, and platelet morphologies.

Chemistry panels composed of 20 tests were performed on serum using a Cobas 6000 analyzer (Roche Diagnostics, Risch-Rotkreuz, Switzerland). Tests in each panel included glucose, blood urea nitrogen, creatinine, creatine kinase, cholesterol, triglycerides, aspartate aminotransferase, alanine aminotransferase, lactic acid dehydrogenase, total bilirubin, gamma-glutamyl transferase, total protein, albumin, alkaline phosphatase, calcium, phosphorous, iron, sodium, potassium, and chloride. CBC and serum chemistry panel results were recorded in the WNPRC Electronic Health Record (EHR) system with species, age, and sex-specific reference intervals provided within the reports generated through the EHR.

Plaque reduction neutralization test ($PRNT_{90}$)

Macaque serum samples were screened for ZIKV neutralizing antibodies utilizing a plaque reduction neutralization test (PRNT) on Vero cells (ATCC #CCL-81). Endpoint titrations of reactive sera, utilizing a 90% cutoff (PRNT90) were performed as previously reported[27,40]

against ZIKV strain H/PF/2013.

Fetal Rhesus Biometric Measurements

Dams were sedated with ketamine hydrochloride (10 mg/kg) for sonographic assessments and amniocentesis. The biparietal diameter (BPD) and head circumference (HC) were measured on an axial image at the level of the hypoechoic thalami, with the echogenic interhemispheric fissure/falx all well visualized[41,42]. The BPD was measured from the outer margin of the near calvarial echo to the inner margin of the deep calvarial echo. The HC was measured circumferentially at the outer margin of the calvaria[42-44]. The abdominal circumference was measured on an axial plane at the level of the stomach and the bifurcation of the main portal vein into the left and right branches, approximately perpendicular to the spine; the abdominal circumference was measured around the outside of the margin of the fetal abdomen[42,45]. The femur length (FL) was measured from the greater trochanter to the lateral condyle along the distal end of the shaft, excluding the femoral head and the distal epiphysis[43]**.** Growth curves were developed[42] for ZIKV-infected monkeys for BPD, HC, and FL. Mean measurements and standard deviations at specified days of gestation in Rhesus macaques were retrieved from Tarantal[35].

Fetal Rhesus Amniocentesis

Under real-time ultrasound guidance, a 22 gauge, 3.5 inch Quincke spinal needle was inserted into the amniotic sac. After 1.5-2 mL of fluid were removed and discarded due to potential maternal contamination, an additional 3-4 mL of amniotic fluid were removed for viral qRT-PCR analysis as described elsewhere[27]. These samples were obtained at the gestational ages specified in Fig. 1A. All fluids were free of any blood contamination.

Magnetic Resonance Imaging

Noninvasive imaging of the fetal brain was performed on isofluorane-anesthetized monkeys on a clinical 3T Magnetic Resonance Imaging (MRI) system (MR750, GE Healthcare, Waukesha, WI). T1 and T2-weighted axial and sagittal images were acquired. T2-weighted axial images were acquired with a single shot fast spin echo (SSFSE) sequence. Scan protocol for Supplementary Fig. 4A: respiratory gated multislice 2D acquisition; TE/TR = 141 / 2526 ms; Slice thickness: 2 mm; acquired spatial resolution = 1.25 mm x 1.25 mm; receiver bandwidth = 651 Hz/pixel. For Supplementary Fig. 4B, T1-weighted axial images were acquired with a multiecho spoiled gradient echo sequence. The scan protocol for respiratory gated 3D acquisition under isoflurane anesthesia was iterative decomposition with echo asymmetry and least-squares estimation (IDEAL) processing for reconstruction of in-phase images from 8 echoes; 2 shots, 4 echoes each shot; flip angle = 15 deg; TE min = 1.6 ms; TR = 15.4 ms; Slice thickness: 1 mm; acquired spatial resolution = 1.1 mm x 1.1 mm; receiver bandwidth = 488 Hz/pixel. Animals were intubated for anesthesia under ketamine sedation, and imaging sessions lasted for approximately 1 hour.

Viral RNA isolation from urine, amniotic fluid, and oral/vaginal swabs

RNA was isolated from maternal and fetal plasma and PBMC, urine, amniotic fluid, and oral and vaginal swabs using the Viral Total Nucleic Acid Purification Kit (Promega, Madison, WI) on a Maxwell 16 MDx instrument as previously reported[27].

Viral RNA isolation from fetal and maternal tissues

Fetal and maternal tissues were processed with RNAlater® (Invitrogen, Carlsbad, CA) according to the manufacturer protocols. Viral RNA was isolated from the tissues using the

Maxwell 16 LEV simplyRNA Tissue Kit (Promega, Madison, WI) on a Maxwell 16 MDx instrument (Promega, Madison, WI). A range of 20-40 mg of each tissue was homogenized using homogenization buffer from the Maxwell 16 LEV simplyRNA Tissue Kit, the TissueLyser (Qiagen, Hilden, Germany) and two 5 mm stainless steel beads (Qiagen, Hilden, Germany) in a 2 ml snapcap tube, shaking twice for 3 minutes at 20 Hz each side. The isolation was continued according to the Maxwell 16 LEV simplyRNA Tissue Kit protocol, and samples were eluted into 50 µl RNase free water.

Quantitative reverse transcription PCR (qRT-PCR)

Viral RNA isolated from plasma, urine, oral swabs, amniotic fluid, and maternal or fetal tissues was quantified by qRT-PCR using modified primers and probe adapted from Lanciotti *et al.*[46] as previously described[40]. The SuperScript III Platinum one-step quantitative RT-PCR system was used (Invitrogen, Carlsbad, CA) on the LightCycler 480 instrument (Roche Diagnostics, Indianapolis, IN). Assay probes were used at final concentrations of 600 nM and 100 nM respectively, along with 150 ng random primers (Promega, Madison, WI). Conditions and methods were as previously described[27]. Tissue viral loads were calculated per mg of tissue.

Cesarean Section and Tissue Collection (Necropsy)

At ~155 days gestation, fetal and maternal tissues were surgically removed at laparotomy. These were survival surgeries for the dams. The entire conceptus within the gestational sac (fetus, placenta, fetal membranes, umbilical cord, and amniotic fluid) was collected and submitted for necropsy. The fetus was euthanized with an overdose of sodium pentobarbitol (50 mg/kg). Tissues were carefully dissected using sterile instruments that were changed between each organ and tissue type to minimize possible cross contamination. Each organ/tissue was evaluated grossly *in situ*, removed with sterile instruments, placed in a sterile culture dish, and sectioned for histology, viral burden assay, or banked for future assays. Sampling priority for small or limited fetal tissue volumes (e.g., thyroid gland, eyes) was vRNA followed by histopathology, so not all tissues were available for both analyses. Sampling of all major organ systems and associated biological samples included the CNS (brain, spinal cord, eyes), digestive, urogenital, endocrine, musculoskeletal, cardiovascular, hematopoietic, and respiratory systems as well as amniotic fluid, gastric fluid, bile, and urine. A comprehensive listing of all specific tissues collected and analyzed is presented in Supplemental Figs. S5 and S6.

Biopsies of the placental bed (uterine placental attachment site containing deep decidua basalis and myometrium), maternal liver, spleen, and a mesenteric lymph node were collected aseptically during surgery into sterile petri dishes, weighed, and further processed for viral burden and when sufficient sample size was obtained, histology. Maternal decidua was dissected from the maternal surface of the placenta.

Histology

Tissues were fixed in 10% neutral buffered formalin for 14 days and transferred into 70% ethanol until routinely processed and embedded in paraffin. Paraffin sections (5 µm) were stained with hematoxylin and eosin (H&E). Pathologists were blinded to vRNA findings when tissue sections were evaluated microscopically. Lesions in each tissue were described and scored for severity as shown in Supplemental Fig. S6, and assigned morphologic diagnoses assigned as listed in Supplemental Item S7. Photomicrographs were obtained using a bright light microscope Olympus BX43 and Olympus BX46 (Olympus Inc., Center Valley, PA) with attached Olympus DP72 digital camera (Olympus Inc.) and Spot Flex 152 64 Mp camera (Spot Imaging), and captured using commercially available image-analysis software (cellSens

Dimension^{R}, Olympus Inc. and spot software 5.2).

For immunohistochemistry, tissues were fixed in 4% paraformaldehyde/PBS overnight then paraffin embedded. 5 µm sections were cut and deparaffinized. Antigen retrieval was accomplished by incubation in heated (95°C) 10 mM citrate buffer (pH 6.0) plus 0.05% Tween-20. The sections were blocked with 5% normal donkey serum for 1 hour at room temp then incubated overnight at 4°C with rabbit anti Zika NS2B 1:100 (GeneTex GTX133308, Irvine, CA) and mouse anti-CD163 1:100 (Novus, NB110-40686, Littleton, CO) or comparable control IgGs (Santa Cruz, Santa Cruz CA). Sections were rinsed with TBS + tween-20 (TBST) 3x and incubated with the appropriate secondary antibodies; donkey anti-rabbit Alexa 647 (1:5000), donkey anti-mouse Alexa 488 (1:2500) for 1 hour at room temperature (Jackson ImmunoResearch Laboratories, West Grove, PA). Sections were washed (3x TBST), exposed to DAPI and mounted with Aqua Poly Seal (Polysciences Inc, Warrington, PA). Sections were evaluated on a Leica SP8 confocal microscope.

Data availability

Primary data that support the findings of this study are available at the Zika Open-Research Portal (https://zika.labkey.com). ZIKV H.sapiens-tc/FRA/2013/FrenchPolynesia-3328 sequence data have been deposited in the Sequence Read Archive (SRA) with accession code SRP072852. The authors declare that all other data supporting the findings of this study are available within the article and its supplementary information files, or from the corresponding author upon request.

ACKNOWLEDGEMENTS
We thank the WNPRC Veterinary, Scientific Protocol Implementation, and Pathology Services staff for assistance with animal procedures, including breeding, ultrasound monitoring, and sample collection, and Ms. Rebecca Black for editorial assistance. We thank Adam Ericsen, Jenna Kropp, and Jiro Wada for help in figure design and illustration. This work was supported by NIH grants R01 AI107157-01A1 to T.G.G., R01AI116382-01A1S1 to D.H.O., DP2HD075699 to S.R.P. and P51 OD011106 to the WNPRC. This research was conducted in part at a facility constructed with support from Research Facilities Improvement Program grant numbers RR15459-01 and RR020141-01. The content is solely the responsibility of the authors and does not necessarily represent the official views of ORIP or the NIH.

COMPETING FINANCIAL INTERESTS

The authors declare no competing financial interests.

AUTHOR CONTRIBUTIONS

All contributing authors have agreed to the submission of this manuscript for publication. D.H.O., T.C.F., J.E.O., M.T.A., E.L.M., T.G.G., S.L.O. and D.M.D. designed the experiments. T.G.G., S.M.N., K.A.A., D.H.O., D.M.D., E.L.M., A.F.T. and T.C.F. drafted the manuscript. M.T.A. and J.E.O. provided and prepared viral stocks and performed plaque reduction neutralizing test assays. K.M.A., S.K., and S.C. performed fetal ultrasound examinations and amniocenteses. A.M.W., G.L.B. and T.C.F. performed viral load assays. K.L.W., L.J.V, and E.G.R. performed immunophenotyping assays. G.J.W., B.W., J.M.H., S.M.N., M.S.M., M.E.B., M.N.R., C.M.N. and D.M.D. coordinated and processed macaque samples for distribution for all subsequent assays. J.P., N.S.D., H.A.S., S.C., and J.M.H., coordinated the macaque infections, sampling, and performed CBC analysis, serum chemistry preparations, and serum optimization. J.P. and M.L.S. coordinated the animal procedures and helped perform ultrasound examinations on the pregnant macaques. P.J.T., O.E.W., and K.M.J. conducted MRI analyses and interpreted data. A.F.T., K.A.A., S.A.A., E.L.M., S.C., B.W., S.M.N., and T.G.G. analyzed and interpreted fetal growth data. H.A.S., L.B.C.T., and S.S. evaluated pathology slides. T.H.T. and G.J.W. conducted immunohistochemical tissue analyses. J.A.E., M.A.M. and S.R.P. performed the plasmablast experiments.

FIGURE LEGENDS

Figure 1 Study layout and viral RNA burden in pregnant rhesus fluids. (a) Schematic representation of the timeline of infection, sampling for maternal viral burden, and experimental cesarean section, for all animals in the study. Animals received a ZIKV challenge in the first or late second/early third trimesters of pregnancy, and blood and other fluid samples were collected according to the schedule indicated in detail in supplemental Fig. S1. (**b**) ZIKV viral load in pregnant macaque fluids. Viral RNA loads (vRNA copies/ml) measured in plasma, urine, saliva, and amniotic fluid presented individually for the four pregnant animals. The day post-inoculation is indicated below each graph, and gestational age (days) for each animal is indicated above (term = 165±10 days). Limit of assay quantification is 100 copies/mL. Limit of detection is 33 copies/mL. Colors for individual animals are continued through Figs. 2-4 and in the Supplementary Figures.

Figure 2 Maternal viral control and immune responses to ZIKV inoculation. (**a)** Peripheral blood plasma viremia in pregnant macaques infected with ZIKV. Results are shown for animals infected at 38 days gestation (animal 827577, Dark Blue), 31 days gestation (animal 660875, Light Blue), 103 days gestation (animal 357676, Orange) or 118 days gestation (animal 598248, Red). The day of gestation is estimated +/- 2 days. Grey tracings represent viremia in nonpregnant/male rhesus monkeys infected with the identical dose and strain of ZIKV in a previous study[27]. The horizontal line indicates the quantitative limit of detection. (**b)** Peripheral blood cell response to infection. Absolute numbers of Ki67+ NK cells or CD8+TEM cells are presented as a percentage relative to baseline set at 100%, with first trimester and third trimester animals represented in the same colors as presented in Fig. 1A. (**c)** Plasmablast expansion over time from each pregnant animal. The plasmablast expansions of two nonpregnant animals from Dudley *et al* [27] are shown as grey lines. (**d)** $PNRT_{90}$ titers for pregnant animals. Data from nonpregnant animals from Dudley *et al*[27] are shown as grey bars.

Figure 3 Fetal growth following ZIKV infection**. (a**) Representative ultrasound images of FL, BPD, and HC are shown. (**b**) Growth data for FL, BPD, and HC obtained from fetal ultrasound examinations during the last month of gestation are presented as individual symbols around the mean (solid black line) data from Tarantal[35] with specific colors as in Fig. 1. One, two, or three standard deviations from the mean are shown as grey lines above and below the mean. All data from across gestation is presented in Supplementary Fig. S3. (**c-f)** The predicted gestational age (pGA) from each of the pregnancies as described by Tarantal[35] is plotted against the day of gestation estimated from breeding activity and animal menstrual records. The pGA was derived from the average of BPD+FL (dashed lines), or the HC (solid lines).

Figure 4 Maternal and fetal viral burden and histopathology analyses. (**a**) Graph of fetal and maternal vRNA burden. Tissues for specific dams and their respective fetuses with detectable vRNA are shown on the x-axis. The y-axis indicates vRNA copy number/mg tissue. The bars indicating vRNA levels are color coded as in Figs. 1-3. All tissues analyzed are presented in Supplementary Fig. S5. (**b**) Hematoxylin and Eosin (H&E) staining of selected tissues. Maternal spleen, 660875: increased neutrophils (arrows) throughout splenic sinusoids. Maternal decidua, 827577: multifocal stromal, intravascular, and perivascular inflammation (arrows). Placenta, 660875: moderate multifocal necrosis and loss of trophoblastic epithelium (+) with viable and degenerative neutrophils (arrows) between villi (*) and throughout the intervillous space.

Chorionic membrane, 598248: diffuse suppurative inflammation throughout the chorionic membrane (ch) with rare single neutrophils (arrows) within the overlying amnion. Amniotic membrane, 598248: scattered neutrophils within the amniotic basement membrane and underlying perivascular stroma. Umbilical cord, 660875: segmental thrombosis (*) with entrapped neutrophils (arrows). Fetal eye (ciliary body pars plana), 660875: are mature neutrophils scattered throughout the stroma of the ciliary body. Fetal lung, 660875: fetal squamous cells (*) and neutrophils (arrows) admixed with fibrin within alveolar spaces. (**c**) Semiquantitative scoring of histologic lesions in maternal and fetal tissues. The colors represent tissues from individual animals as presented in Fig. 1. Scale: 0 = normal, 1 = minimal pathology, 2 = mild pathology, 3 = moderate pathology, 4 = severe pathology. Only tissues scoring 1-4 are presented; Supplementary Fig. S6B summarizes results in all evaluated tissues. (**d**) Immunofluorescent staining for ZIKV NS2B (red) and macrophage marker CD163 (green) in fetal axillary lymph node with a high vRNA burden. An H&E serial section of the immunostained region is also presented. The white scale bar = 100 µm. The nonspecific isotype control and additional areas from this same tissue specimen are shown in Supplementary Figure S9.

SUPPLEMENTARY FIGURES:

Supplementary Figure S1. Comprehensive sampling experimental timeline for pregnant animals in the current study. Each animal in the study is indicated at the left, color blocks represent when specific samples were collected (e.g., CSF on 43 dpi (81 days gestation) for animal 827577).

Supplementary Figure S2. Complete blood counts (CBCs) and serum chemistries for pregnant macaques infected with ZIKV. Animals were infected with 10^4 PFU of ZIKV. Animals infected in the first trimester are represented by color coding as presented in Figures 1-4. All animals had CBC analysis performed on EDTA blood and chemistry analysis performed on serum at -7, -3, 0, 1-10 and additional indicated dpi. **a.** % lymphocytes, **b.** WBC counts, **c.** RBC counts, **d.** AST blood chemistries, **E.** ALT serum chemistries, **f.** CK serum chemistries.

Supplementary Figure S3. Growth curves of femur length (FL), biparietal diameter (BPD), and head circumference (HC) throughout gestation. Growth curves obtained from fetal ultrasound images are presented as individual lines or symbols with specific colors as in Fig. 1. (**a**) FL, (**b**) BPD (**c**) and HC were determined for the fetuses in this study and plotted against data from Tarantal[35], which is presented as the mean (solid black line) and 1, 2, and 3 standard deviations from the mean as grey lines above and below the mean. The data from the last month of pregnancy are also presented as a magnified view of the scatter of individual data points in Figure 3.

Supplementary Figure S4 Fetal brain imaged by MRI in ZIKV-infected pregnancies. (**a**) T2-weighted axial images of the fetus from dam 660875 at 60 dpi (91 days gestation) acquired with a single shot fast spin echo (SSFSE) sequence. Fluids such as the intraocular fluid, CSF, and amniotic fluid as well as fat appear bright on these images. The brain anatomy appears normal. **(b**) The same fetus acquired with a multiecho spoiled gradient echo sequence.

Supplementary Figure S5. Descriptive diagram showing all maternal and fetal tissues that were sampled at collection.

Supplementary Figure S6. Charts summarizing (**a**) ZIKV RNA copy number scores, and (**b**) histologic evaluation and semiquantitative scoring of all normal and lesioned tissues, presenting all tissues analyzed.

Supplementary Data S7. Morphologic diagnoses from gross and histologic examination of maternal, fetal, and maternal-fetal interface tissues.

Necropsy 598248:

- Placenta: minimal to mild multifocal suppurative and necrotizing placentitis.
- Decidua: minimal lymphocytic and neutrophilic deciduitis.
- Amnion: mild diffuse suppurative amnionitis.
- Chorion: Mild diffuse suppurative chorioamnionitits with multifocal mineralization.
- Spleen, fetus: minimal diffuse splenitis.
- Pancreatic lymph node, fetus: moderate diffuse suppurative lymphadenitis.
- Gastric lymph node, fetus: mild diffuse suppurative lymphadenitis.
- Lungs, fetus: mild diffuse suppurative alveolitis (pneumonia) with intra-alveolar squamous cells and occasional macrophages.
- Liver, fetus: mild suppurative and lymphoplasmacytic cholangiohepatitis and serositis with mild multifocal extramedullary hematopoiesis.

Necropsy 357676:

- Placenta: moderate multifocal suppurative placentitis with thrombosis and multifocal mineralization.
- Decidua: mild multifocal suppurative deciduitis with thrombosis and multifocal mineralization.
- Amnion: Severe diffuse edema with minimal diffuse suppurative amnionitis.
- Chorion: moderate multifocal to diffuse suppurative chorioamnionitis.
- Spleen, maternal: mild suppurative splenitis.
- Axillary lymph node, fetus: minimal suppurative lymphadenitis.
- Inguinal lymph node, fetus: minimal suppurative lymphadenitis.
- Lung, fetus: scattered single intra-alveolar squamous cells and minimal pulmonary edema.
- Pericardium, fetus: mild multifocal nodular lymphoid hyperplasia.
- Liver, fetus: minimal multifocal extramedullary hematopoiesis.
- Buccal mucosa, fetus: mild multifocal ballooning degeneration.

Necropsy 827577:

- Placenta: moderate multifocal suppurative placentitis, multifocal mineralization, and perivascular lymphocytic infiltration.
- Decidua: moderate multifocal suppurative deciduitis.
- Amnion: minimal multifocal suppurative amnionitis, multifocal perivascular lymphocytic infiltration.
- Spleen, maternal: mild diffuse suppurative splenitis.
- Eye, fetus: Minimal lymphocytic iritis, minimal lymphocytic conjunctivitis, mild peripheral retinal and optic nerve gliosis.
- Spleen, fetus: Mild suppurative splenitis.
- Lungs, fetus: moderate intra-alveolar squamous cells.

Necropsy 660875

- Placenta: Moderate multifocal necrosuppurative placentitis.
- Decidua: mild to moderate diffuse suppurative deciduitis.
- Spleen, maternal: moderate diffuse suppurative splenitis with severe multifocal lymphoid hyperplasia with follicular dysplasia.
- Liver, maternal: minimal multifocal periportal lymphosuppurative hepatitis.
- Lymph node, maternal: moderate diffuse lymphoid hyperplasia.
- Umbilical cord, infant: focal fibrin thrombus with intralesional neutrophils.
- Eye, fetus: minimal lymphocytic iritis, moderate neutrophilic cyclitis, minimal lymphocytic conjunctivitis, moderate optic nerve gliosis.
- Spleen, fetus: mild diffuse suppurative splenitis.
- Axillary lymph node, fetus: moderate diffuse suppurative lymphadenitis.
- Submandibular lymph node, fetus: moderate diffuse suppurative lymphadenitis.
- Inguinal lymph node, fetus: moderate diffuse suppurative lymphadenitis.
- Lungs, fetus: Moderate diffuse suppurative alveolitis with intra-alveolar squamous cells.
- Liver, fetus: minimal multifocal suppurative periportal and serosal hepatitis.

Supplementary Figure S8. Panels 1a-c, animal 660875.Panel 1a: Mild infiltration of lymphocytes in the bulbar conjunctival substantia propria (arrow). Panel 1b: Moderate neutrophilic infiltration in the ciliary body stroma (arrows). Panel 1c: Moderate gliosis of the laminar and post-laminar optic nerve characterized by overall hypercellularity of the neuropil especially as indicated by asterisks. Panels 2a-c, animal 827577. Panel 2a: Minimal infiltration of lymphocytes in the bulbar conjunctival substantia propria (arrows). Panel 2b: Normal ciliary body stroma. Panel 2c: Moderate gliosis of the laminar and post-laminar optic nerve characterized by overall hypercellularity of the neuropil especially as indicated by asterisks. Panels 3a-c, animal 357676, and Panels 4a-c, animal 598248. Panels 3a and 4a: Normal bulbar conjunctival substantia propria. Panels 3b and 4b: Normal ciliary body stroma. Panels 3c and 4c: Normal optic nerve.

Supplementary Figure S9. Chart summarizing all maternal and fetal outcomes for each individual pregnancy, including quantitative vRNA burden and semiquantitative histopathology scores.

Supplementary Figure S10. (**a**) Nonspecific immunostaining with control isotypes for ZIKV NS2B and CD163. (**b-c**) Staining of additional fetal axillary lymph node regions. Red immunofluorescence indicates ZIKV+ cells, green immunofluorescence indicates CD163+ cells.

References

1. Musso, D. & Gubler, D.J. Zika Virus. *Clin Microbiol Rev* **29**, 487-524 (2016).
2. Hahn, M.B.*, et al.* Reported Distribution of Aedes (Stegomyia) aegypti and Aedes (Stegomyia) albopictus in the United States, 1995-2016 (Diptera: Culicidae). *J Med Entomol* (2016).
3. Brooks, J.T.*, et al.* Update: Interim Guidance for Prevention of Sexual Transmission of Zika Virus - United States, July 2016. *MMWR Morb Mortal Wkly Rep* **65**, 745-747 (2016).
4. Foy, B.D.*, et al.* Probable non-vector-borne transmission of Zika virus, Colorado, USA. *Emerg Infect Dis* **17**, 880-882 (2011).
5. Hills, S.L.*, et al.* Transmission of Zika Virus Through Sexual Contact with Travelers to Areas of Ongoing Transmission - Continental United States, 2016. *MMWR Morb Mortal Wkly Rep* **65**, 215-216 (2016).
6. Rowland, A., Washington, C.I., Sheffield, J.S., Pardo-Villamizar, C.A. & Segars, J.H. Zika virus infection in semen: a call to action and research. *J Assist Reprod Genet* **33**, 435-437 (2016).
7. Deckard, D.T.*, et al.* Male-to-Male Sexual Transmission of Zika Virus--Texas, January 2016. *MMWR Morb Mortal Wkly Rep* **65**, 372-374 (2016).
8. Davidson, A., Slavinski, S., Komoto, K., Rakeman, J. & Weiss, D. Suspected Female-to-Male Sexual Transmission of Zika Virus - New York City, 2016. *MMWR Morb Mortal Wkly Rep* **65**, 716-717 (2016).
9. Barzon, L.*, et al.* Infection dynamics in a traveller with persistent shedding of Zika virus RNA in semen for six months after returning from Haiti to Italy, January 2016. *Euro Surveill* **21**(2016).
10. Schuler-Faccini, L.*, et al.* Possible Association Between Zika Virus Infection and Microcephaly - Brazil, 2015. *MMWR Morb Mortal Wkly Rep* **65**, 59-62 (2016).
11. Cauchemez, S.*, et al.* Association between Zika virus and microcephaly in French Polynesia, 2013-15: a retrospective study. *Lancet* **387**, 2125-2132 (2016).
12. Soares de Oliveira-Szejnfeld, P., *et al.* Congenital Brain Abnormalities and Zika Virus: What the Radiologist Can Expect to See Prenatally and Postnatally. *Radiology* **281**, 203-218 (2016).
13. Oliveira Melo, A.S.*, et al.* Zika virus intrauterine infection causes fetal brain abnormality and microcephaly: tip of the iceberg? *Ultrasound Obstet Gynecol* **47**, 6-7 (2016).
14. Brasil, P.*, et al.* Zika Virus Infection in Pregnant Women in Rio de Janeiro. *N Engl J Med* **375**, 2321-2334 (2016).
15. Martines, R.B.*, et al.* Pathology of congenital Zika syndrome in Brazil: a case series. *Lancet* **388**, 898-904 (2016).
16. Noronha, L., Zanluca, C., Azevedo, M.L., Luz, K.G. & Santos, C.N. Zika virus damages the human placental barrier and presents marked fetal neurotropism. *Mem Inst Oswaldo Cruz* **111**, 287-293 (2016).
17. de Paula Freitas, B.*, et al.* Ocular Findings in Infants With Microcephaly Associated With Presumed Zika Virus Congenital Infection in Salvador, Brazil. *JAMA Ophthalmol* (2016).
18. Moore, C.A.*, et al.* Characterizing the Pattern of Anomalies in Congenital Zika Syndrome for Pediatric Clinicians. *JAMA Pediatr* (2016).
19. van der Linden, V.*, et al.* Congenital Zika syndrome with arthrogryposis: retrospective case series study. *BMJ* **354**, i3899 (2016).
20. Leal, M.C.*, et al.* Hearing Loss in Infants with Microcephaly and Evidence of Congenital

Zika Virus Infection - Brazil, November 2015-May 2016. *MMWR Morb Mortal Wkly Rep* **65**, 917-919 (2016).
21. Costello, A.*, et al.* Defining the syndrome associated with congenital Zika virus infection. *Bull World Health Organ* **94**, 406-406A (2016).
22. Miranda-Filho Dde, B.*, et al.* Initial Description of the Presumed Congenital Zika Syndrome. *Am J Public Health* **106**, 598-600 (2016).
23. Franca, G.V.*, et al.* Congenital Zika virus syndrome in Brazil: a case series of the first 1501 livebirths with complete investigation. *Lancet* **388**, 891-897 (2016).
24. Meaney-Delman, D.*, et al.* Prolonged Detection of Zika Virus RNA in Pregnant Women. *Obstet Gynecol* **128**, 724-730 (2016).
25. Driggers, R.W.*, et al.* Zika Virus Infection with Prolonged Maternal Viremia and Fetal Brain Abnormalities. *N Engl J Med* (2016).
26. van der Eijk, A.A.*, et al.* Miscarriage Associated with Zika Virus Infection. *N Engl J Med* **375**, 1002-1004 (2016).
27. Dudley, D.M.*, et al.* A rhesus macaque model of Asian-lineage Zika virus infection. *Nat Commun* **7**, 12204 (2016).
28. Osuna, C.E.*, et al.* Zika viral dynamics and shedding in rhesus and cynomolgus macaques. *Nature medicine* **22**, 1448-1455 (2016).
29. Abbink, P.*, et al.* Protective efficacy of multiple vaccine platforms against Zika virus challenge in rhesus monkeys. *Science* **353**, 1129-1132 (2016).
30. Enders, A.C. Implantation in the macaque: expansion of the implantation site during the first week of implantation. *Placenta* **28**, 794-802 (2007).
31. Blankenship, T.N., Enders, A.C. & King, B.F. Trophoblastic invasion and the development of uteroplacental arteries in the macaque: immunohistochemical localization of cytokeratins, desmin, type IV collagen, laminin, and fibronectin. *Cell Tissue Res* **272**, 227-236 (1993).
32. Bondarenko, G.I.*, et al.* Passive immunization against the MHC class I molecule Mamu-AG disrupts rhesus placental development and endometrial responses. *J Immunol* **179**, 8042-8050 (2007).
33. Adams Waldorf, K.M., Rubens, C.E. & Gravett, M.G. Use of nonhuman primate models to investigate mechanisms of infection-associated preterm birth. *BJOG* **118**, 136-144 (2011).
34. Adams Waldorf, K.M.*, et al.* Fetal brain lesions after subcutaneous inoculation of Zika virus in a pregnant nonhuman primate. *Nature medicine* **22**, 1256-1259 (2016).
35. Tarantal, A.F. Ultrasound Imaging in Rhesus (*Macaca mulatta*) and Long-tailed (*Macaca fascicularis*) Macaques: Reproductuve and Research Applications. in *The Laboratory Primate* (ed. Wolfe-Coote, S.) 317-352 (Elsevier, London, 2005).
36. Tarantal, A.F. & Hendrickx, A.G. Prenatal Growth in the Cynomolgus and Rhesus Macaque (*Macaca fascicularis* and *Macaca mulatta*): A Comparison by Ultrasonography. *Am J Primatol* **15**, 309-323 (1988).
37. Mlakar, J.*, et al.* Zika Virus Associated with Microcephaly. *N Engl J Med* **374**, 951-958 (2016).
38. van der Linden, V.*, et al.* Description of 13 Infants Born During October 2015-January 2016 With Congenital Zika Virus Infection Without Microcephaly at Birth - Brazil. *MMWR Morb Mortal Wkly Rep* **65**, 1343-1348 (2016).
39. Pomplun N, Weisgrau KL, Evans DT, Rakasz EG. OMIP-028: Activation Panel for Rhesus Macaque NK Cell Subsets. *Cytometry Part A□: the journal of the International Society for Analytical Cytology*. 2015;87(10):890-893. doi:10.1002/cyto.a.22727.
40. Aliota, M.T.*, et al.* Heterologous Protection against Asian Zika Virus Challenge in

Rhesus Macaques. *PLoS Negl Trop Dis* **10**, e0005168 (2016).
41. Shepard, M. & Filly, R.A. A standardized plane for biparietal diameter measurement. *J Ultrasound Med* **1**, 145-150 (1982).
42. Tarantal, A.F. & Hendrickx, A.G. Use of ultrasound for early pregnancy detection in the rhesus and cynomolgus macaque (*Macaca mulatta* and *Macaca fascicularis*). *J Med Primatol* **17**, 105-112 (1988).
43. Ville, Y. & Nyberg, D.A. Growth, Doppler, and Fetal Assessment. in *Diagnostic Imaging of Fetal Anomalies* (eds. Nyberg, D.A., McGahan, J.P., Pretorius, D.H. & Pilu, G.) 32-34 (Lippincott Williams & Wilkins, Philadelphia, PA, 2003).
44. Altman, D.G. & Chitty, L.S. New charts for ultrasound dating of pregnancy. *Ultrasound Obstet Gynecol* **10**, 174-191 (1997).
45. Deter, R.L., Harrist, R.B., Hadlock, F.P. & Carpenter, R.J. The use of ultrasound in the assessment of normal fetal growth: a review. *J Clin Ultrasound* **9**, 481-493 (1981).
46. Lanciotti, R.S.*, et al.* Genetic and serologic properties of Zika virus associated with an epidemic, Yap State, Micronesia, 2007. *Emerg Infect Dis* **14**, 1232-1239 (2008).

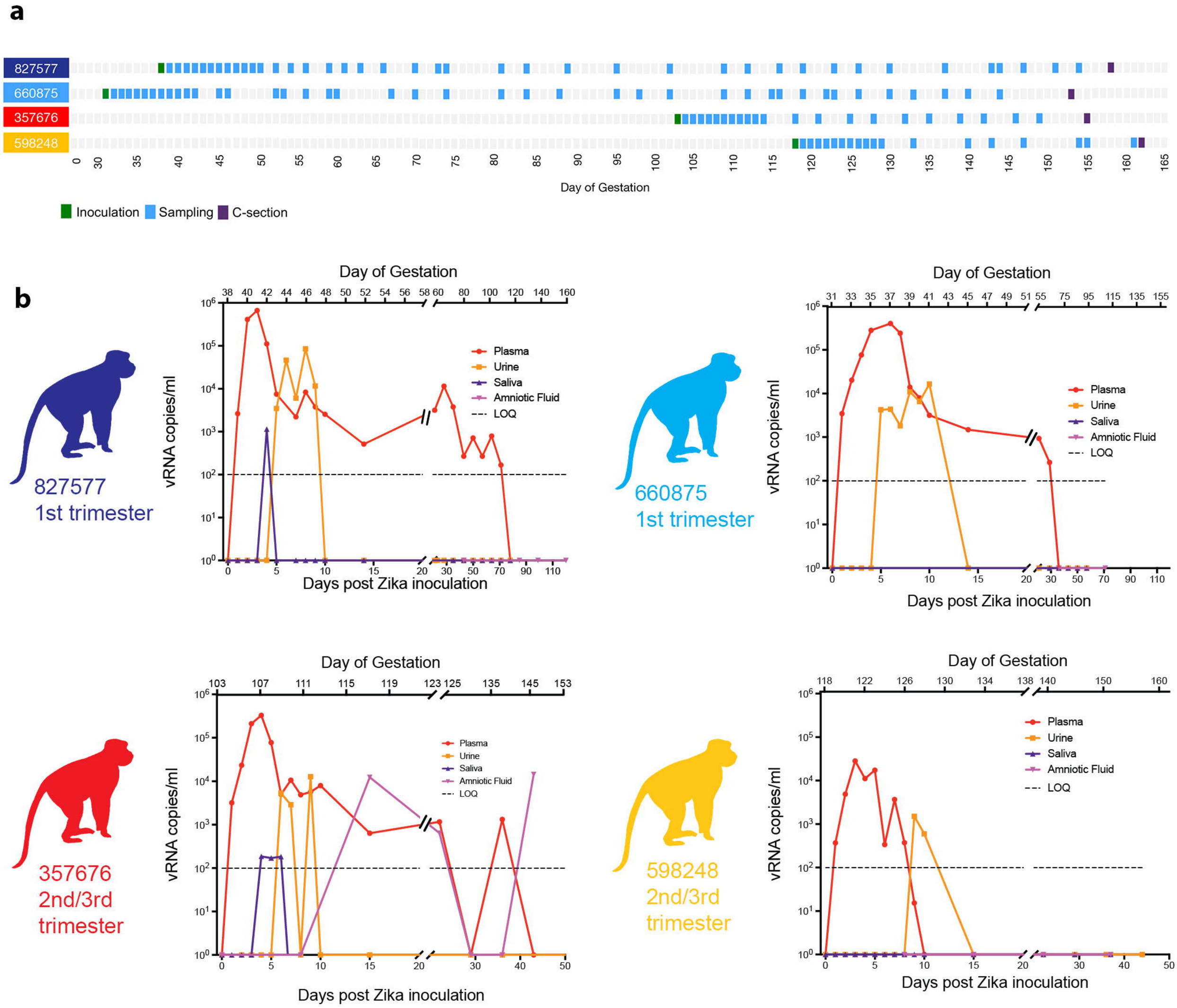
a
827577
660875
357676
598248
Day of Gestation
Inoculation
Sampling
C-section
b
827577
1st trimester
660875
1st trimester
357676
2nd/3rd
trimester
598248
2nd/3rd
trimester
vRNA copies/ml
Days post Zika inoculation
Plasma
Urine
Saliva
Amniotic Fluid
LOQ

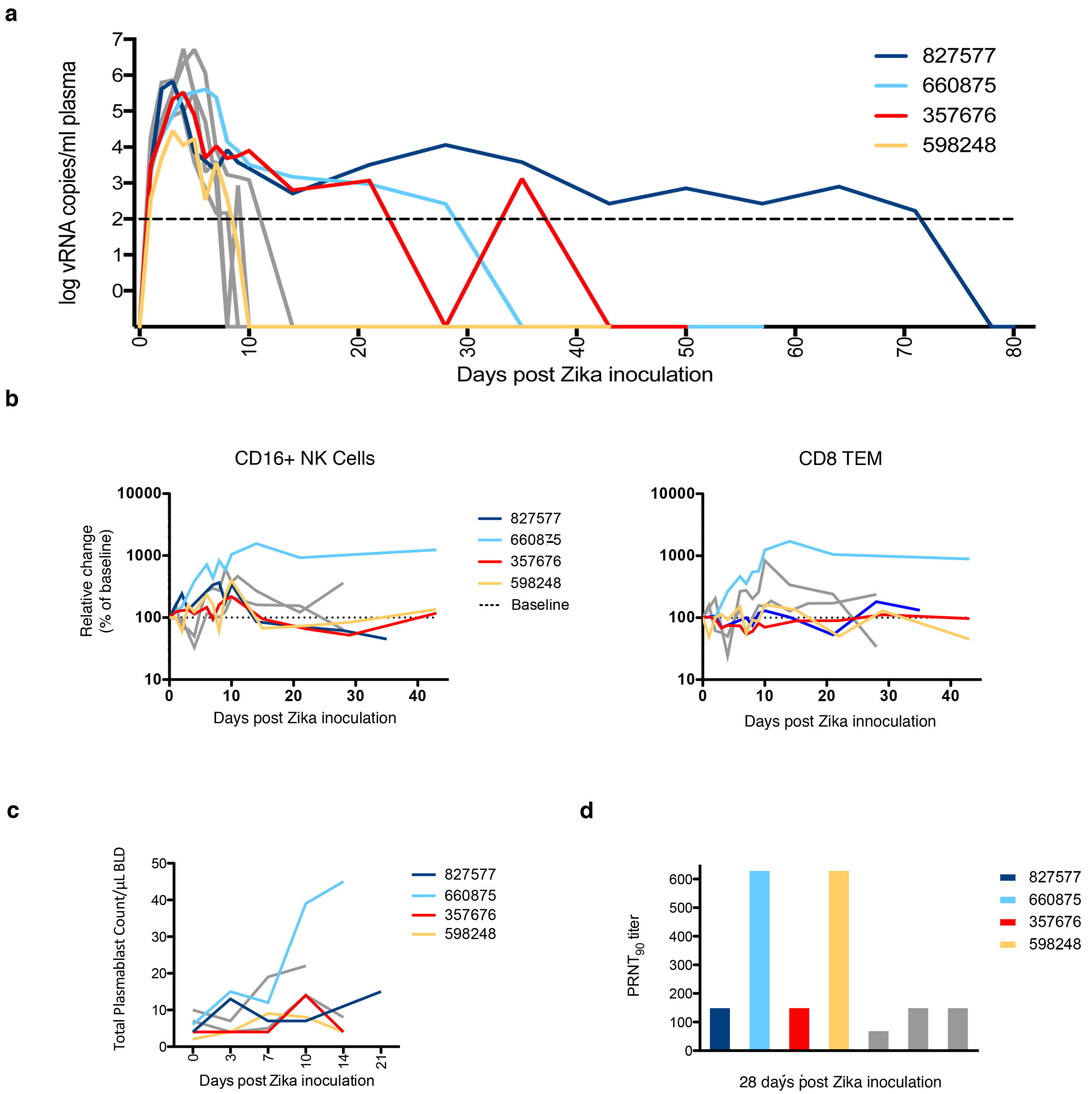
a
log vRNA copies/ml plasma
Days post Zika inoculation
827577
660875
357676
598248
b
CD16+ NK Cells
Relative change (% of baseline)
Days post Zika inoculation
827577
660875
357676
598248
Baseline
CD8 TEM
Days post Zika innoculation
c
Total Plasmablast Count/µL BLD
Days post Zika inoculation
827577
660875
357676
598248
d
PRNT90 titer
28 days post Zika inoculation
827577
660875
357676
598248

a

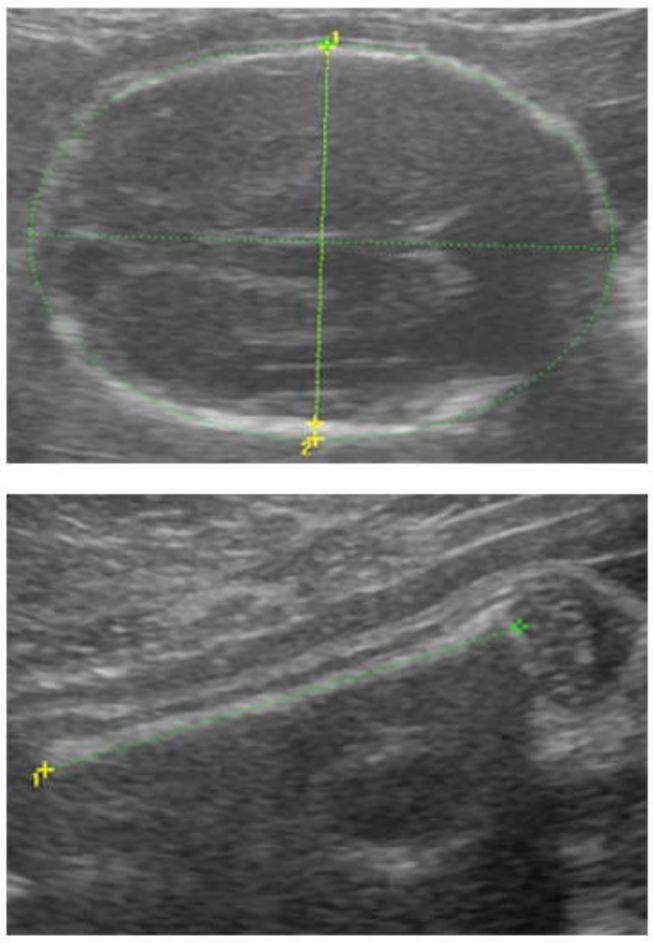

b

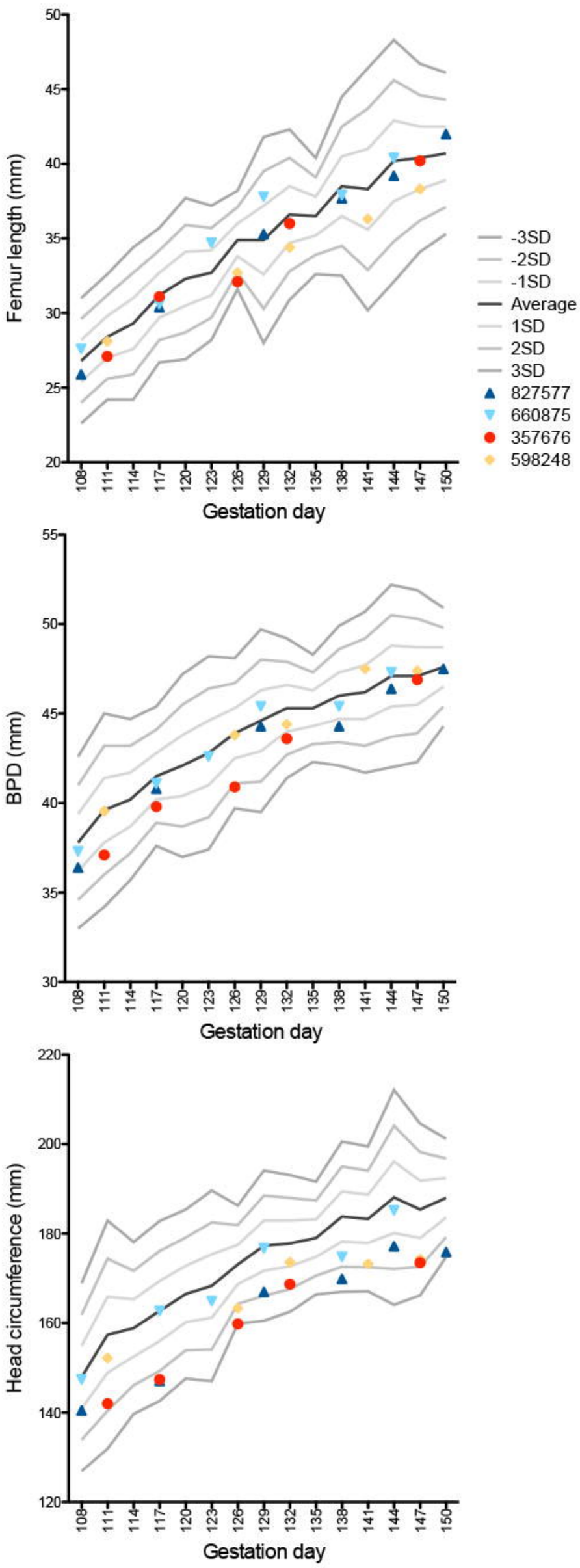
Femur length (mm)
Gestation day
BPD (mm)
Gestation day
Head circumference (mm)
Gestation day
-3SD
-2SD
-1SD
Average
1SD
2SD
3SD
827577
660875
357676
598248

c

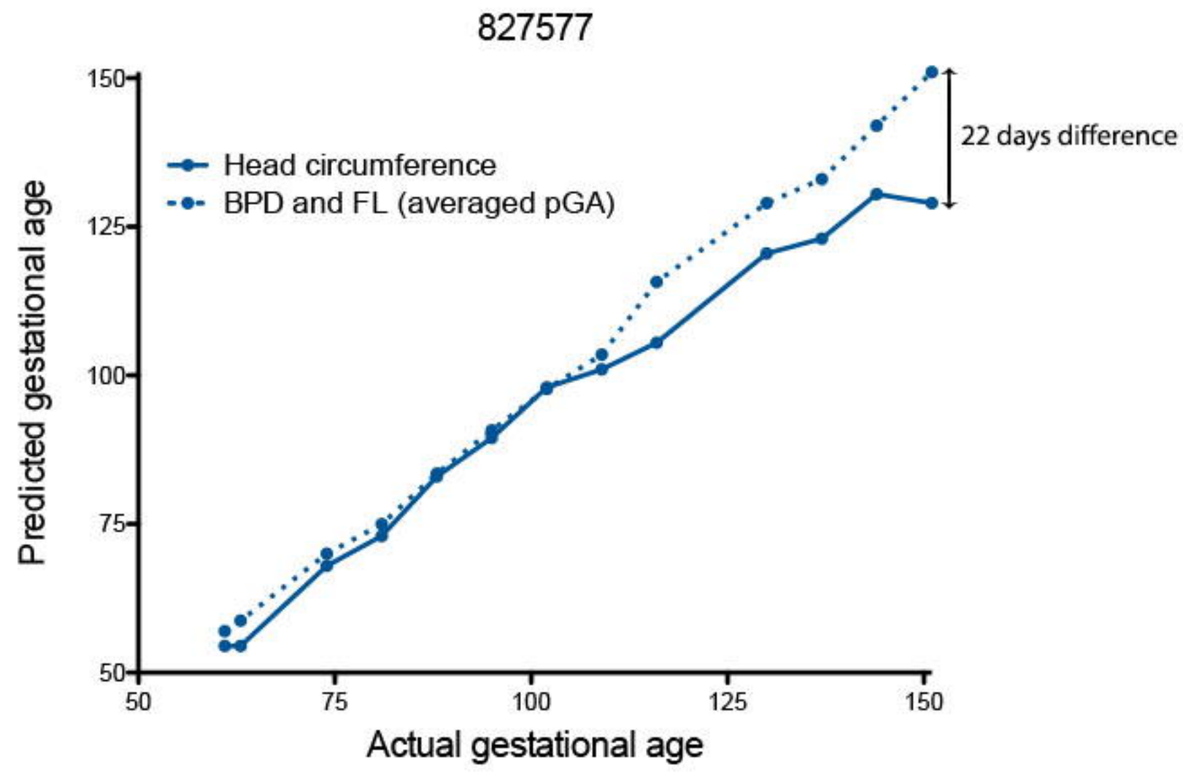
827577
Head circumference
BPD and FL (averaged pGA)
22 days difference
Predicted gestational age
Actual gestational age

d

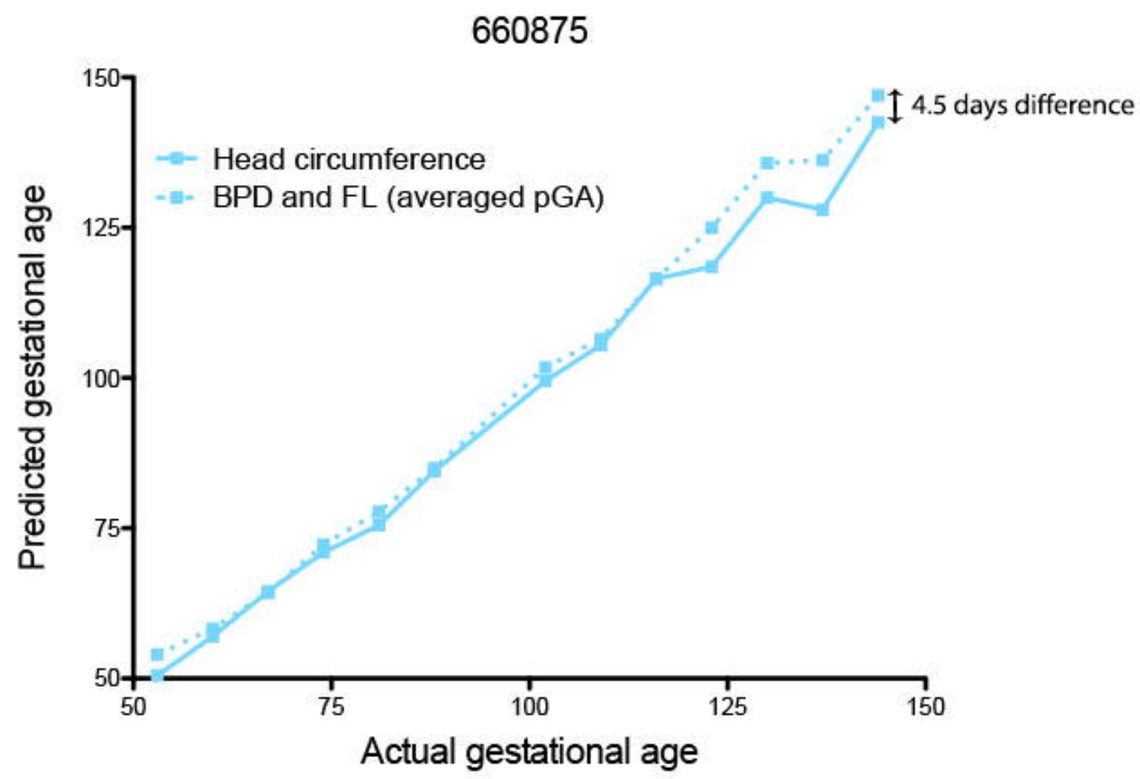
660875
Head circumference
BPD and FL (averaged pGA)
4.5 days difference
Predicted gestational age
Actual gestational age

e

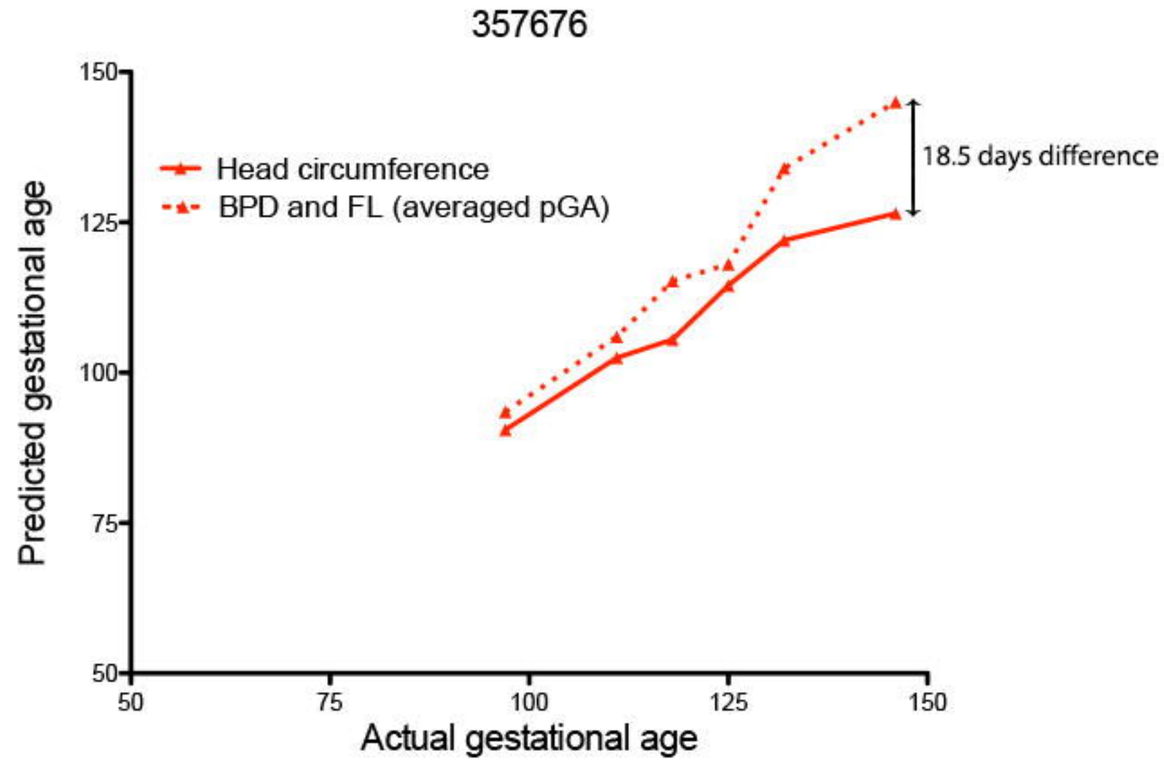
357676
Head circumference
BPD and FL (averaged pGA)
18.5 days difference
Predicted gestational age
Actual gestational age

f

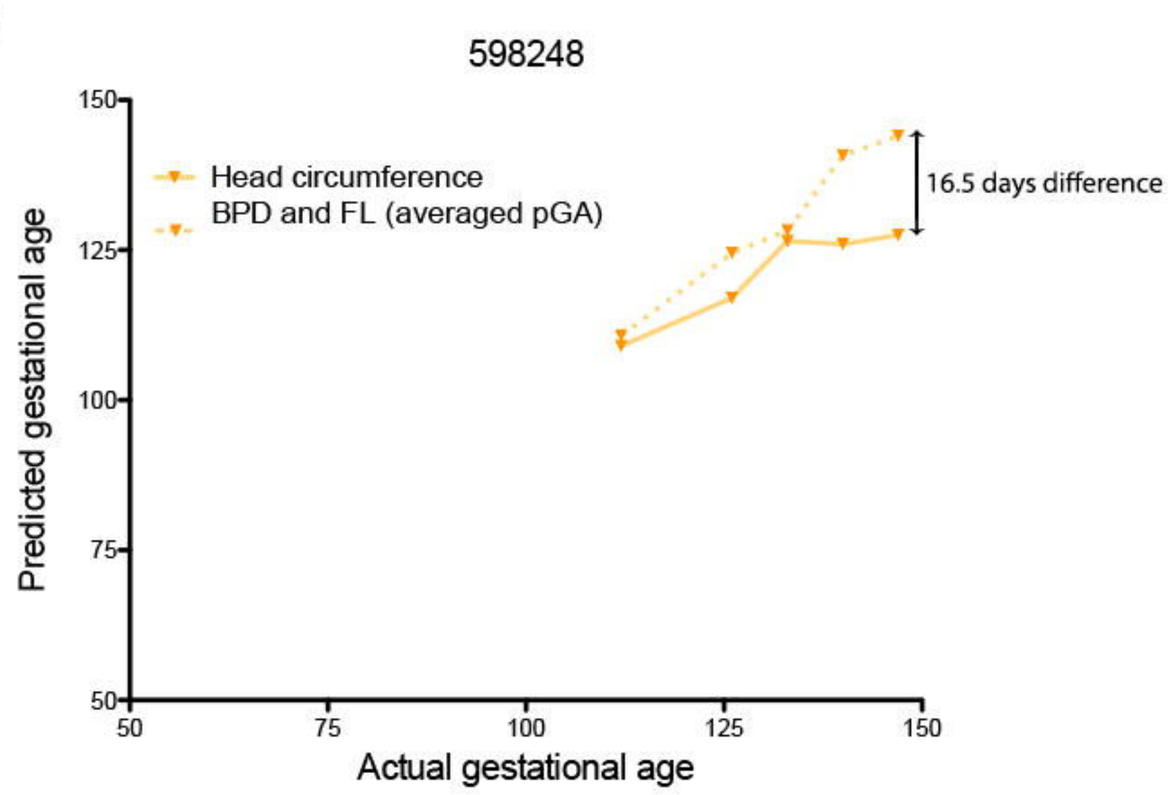
598248
Head circumference
BPD and FL (averaged pGA)
16.5 days difference
Predicted gestational age
Actual gestational age

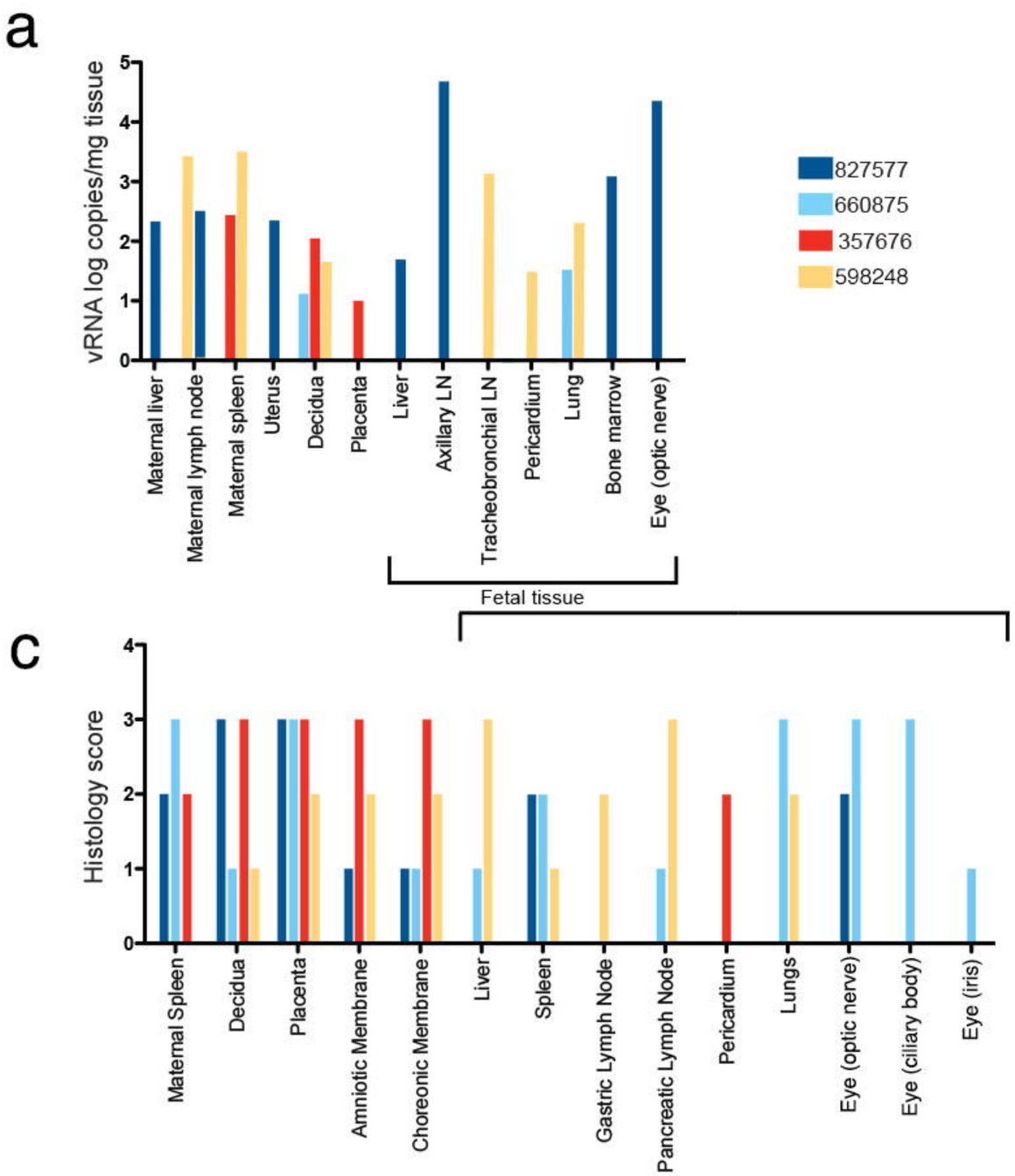
a
vRNA log copies/mg tissue
0
1
2
3
4
5
827577
660875
357676
598248
Maternal liver
Maternal lymph node
Maternal spleen
Uterus
Decidua
Placenta
Liver
Axillary LN
Tracheobronchial LN
Pericardium
Lung
Bone marrow
Eye (optic nerve)
Fetal tissue
c
Histology score
0
1
2
3
4
Maternal Spleen
Decidua
Placenta
Amniotic Membrane
Choreonic Membrane
Liver
Spleen
Gastric Lymph Node
Pancreatic Lymph Node
Pericardium
Lungs
Eye (optic nerve)
Eye (ciliary body)
Eye (iris)

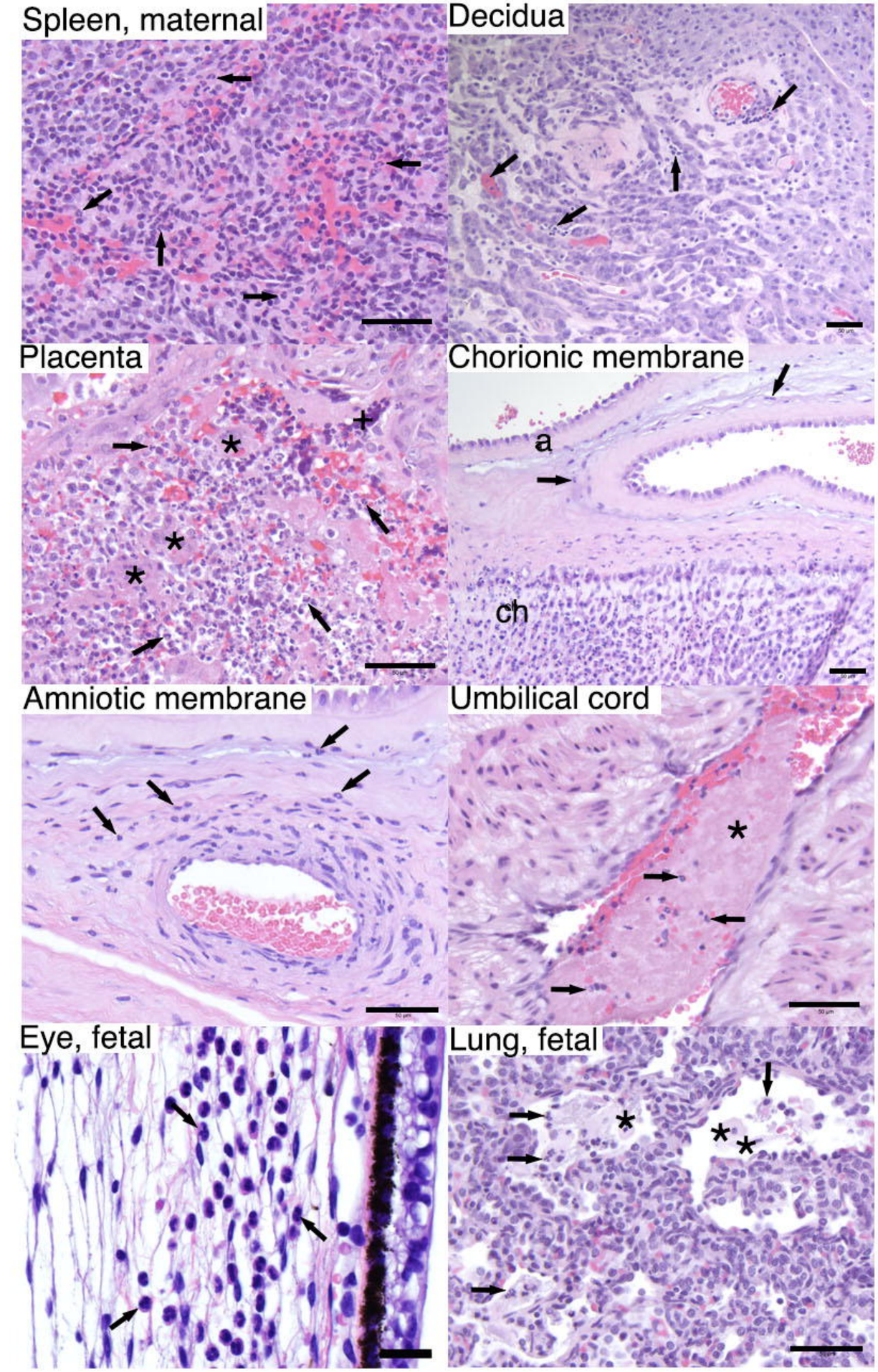
b
Spleen, maternal
Decidua
Placenta
Chorionic membrane
a
ch
Amniotic membrane
Umbilical cord
Eye, fetal
Lung, fetal